NATIONAL AERONAUTICS AND SPACE ADMINISTRATION

Technical Report No. 32-864

Mass-Retention Measurements in a Binary Compressible Vortex Flow

Thomas J. Pivirotto

JET PROPULSION LABORATORY
CALIFORNIA INSTITUTE OF TECHNOLOGY
PASADENA, CALIFORNIA

June 15, 1966

NATIONAL AERONAUTICS AND SPACE ADMINISTRATION

Technical Report No. 32-864

Mass-Retention Measurements in a Binary Compressible Vortex Flow

Thomas J. Pivirotto

D. R. Bartz, Manager
Research and Advanced Concepts Section

JET PROPULSION LABORATORY
CALIFORNIA INSTITUTE OF TECHNOLOGY
PASADENA, CALIFORNIA

June 15, 1966

Prepared Under Contract No. NAS 7-100
National Aeronautics & Space Administration

CONTENTS

TABLES

FIGURES

ABSTRACT

29513

Confined binary vortex flow fields have been proposed as gaseous-fuel-retention devices for gas-core nuclear reactors. Several such flows have been evaluated in this investigation by measuring the mass flow rate of heavy gas discharging from the vortex tube. Hydrogen and nitrogen were used to generate the vortex flow fields and Freon-13 was used for the heavy gas. An infrared photometer operating at a wavelength of approximately 8.3 μ was developed and used to measure the transient decay of the discharge rate of Freon after an abrupt cutoff of Freon inlet flow. From these measurements the average residence time of the Freon particles in several vortex-tube configurations for several mass flow rates of Freon and hydrogen or nitrogen were determined. The conclusion reached from the results of this investigation was that these particular vortex flow fields do not retain significantly more Freon than would be contained in the same device and under the same conditions of pressure and temperature if no diffusion occurred between the light and heavy species.

I. INTRODUCTION

The maximum potential of a nuclear reactor as a direct source of energy for a rocket motor can only be realized if a means can be found to transfer the energy to the propellant at very high temperatures. This requirement places severe limitations on the technique used to confine the nuclear fuel while the propellant gas flows through the reactor. The simplest technique is one in which the propellant gas flows over fuel-loaded graphite plates, but the performance of this system is limited by the temperature limitations of the plates. Several concepts to overcome this limitation have been suggested in the literature. These concepts generally fall into three categories: those in which a gaseous fuel is separated from the propellant by transparent walls through which the energy is transferred by thermal radiation; those in which a liquified or gaseous fuel is prevented from mixing with the propellant by centrifugal or electromagnetic forces or inertia and the energy is transferred by thermal radiation and conduction; and those in which a gaseous fuel and propellant are first mixed together, then separated by a centrifugal force field after the energy has been transferred by particle collisions between the fission fragments and the propellant molecules.

An example of the latter category, designated as a gaseous-vortex reactor, is presented and partially analyzed in Ref. 1 and is shown schematically in Fig. 1. The gaseous-vortex-reactor concept takes advantage of the strong radial pressure gradient generated by a vortex-type flow to induce diffusion between the light gaseous

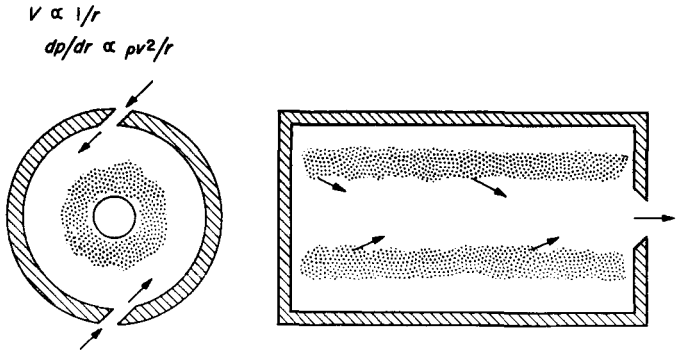

Fig. 1. Schematic of gaseous-vortex-reactor concept

propellant and the much heavier gaseous fuel. This process theoretically results in a concentration of fuel within an annular region of small radial increment. Conceptually, the propellant gas migrates radially inward through the hot, dense, annular cloud of fissioning fuel and then flows axially out through a hole in the center of one end wall. In this gaseous-vortex-reactor concept two requirements are placed on the gas-dynamic flow field.

First, the vortex must retain a mass of gaseous fuel equivalent to a critical mass inside the reactor while allowing the propellant gas (i.e., hydrogen) to flow through the reactor. In Ref. 1, average gaseous-fuel densities of the order of 10^{18} particles/cc in a vortex tube of volume 0.01 ft^3 and propellant flow rates of the order of 10^{-2} lbm/sec per foot of vortex-tube length were used in the performance analysis. This gaseous-fuel retention must be accomplished with an acceptably low gaseous-fuel loss rate. In order to decrease this loss and still maintain the required mass of fuel inside the vortex tube, the average residence time of the fuel particles must be increased. This average residence time relative to the residence time one would expect if no diffusion were occurring between the two species is used to evaluate the various vortex flow fields investigated. Note that if no diffusion were occurring, the gaseous-fuel residence time would be equal to that of the average propellant particle. Hence, the evaluation is based on the ratio of the average residence time of the heavy particles to the average residence time of the light particles. The gaseous-fuel loss rate has been considered in detail with respect to biological hazards, system performance, and economics in Ref. 2.

The second requirement imposed on the gas-dynamic flow field is that it must restrict most of the fuel to an annular cloud located some distance from the cylindrical wall of the tube to reduce the heat-transfer load on this wall. In addition, the radial pressure gradient must prevent the fuel from being convected into the core of the vortex flow field where high axial velocities are expected to occur.

Measurements of the spatial distribution of a gas with a relatively high molecular weight in a binary vortex flow have been reported in Ref. 3 and 4. These measurements qualitatively confirm the theoretical prediction that an annular cloud or region in which the gaseous-fuel density is greater than that at the periphery and center of the axisymmetric flow can exist in a binary vortex. However, these measurements show the maximum heavy-gas (high molecular weight) density to be of the same order of magnitude as the peripheral density, whereas the gaseous-vortex-reactor concept requires the maximum density to be several orders of magnitude greater than that at the periphery. One possible reason for these discouraging results is that the probes used to sample the binary mixture to determine the radial distribution of the heavy gas disturbed the flow to the extent of reducing the maximum gas density in the cloud.

Questions concerning the detailed effect of such probes on rotating flows are difficult to resolve; therefore, an independent experimental means of evaluating vortex tubes as gas-separating devices was sought. The technique used here was designed to qualitatively measure the total mass of heavy gas retained in the vortex tube used for the detailed measurements reported in Ref. 4 for various flow rates of Freon-13 and hydrogen or nitrogen. From these measurements the average residence time of the heavy-gas particles in the vortex tube has been deduced. A second purpose was to find a configuration and/or set of flow conditions that would retain orders-of-magnitude more heavy gas than could be expected if no separation were occurring.

The technique employed an optical probe to monitor the flow of the heavy gas, Freon-13 (chlorotrifluoromethane), leaving the vortex tube. The total retained mass was then determined by integrating the Freon flow rate as a function of time starting from the instant the Freon flow into the vortex tube was abruptly stopped. Both hydrogen and nitrogen were used as the propellant-simulating gas, with the flow rates ranging from 3.95×10^{-3} to 4.93×10^{-2} lbm/sec for hydrogen and from 1.41×10^{-2} to 1.02×10^{-1} lbm/sec for nitrogen. The Freon-13 flow rate was varied between 1.52×10^{-4} and 3.94×10^{-3} lbm/sec. Three basically different configurations were used, including the configuration used to make the detailed probing measurements reported in Ref. 4.

The Freon was premixed with the hydrogen or nitrogen and the mixture then injected into the vortex tube or pure Freon was injected directly into the vortex chamber at the center of the closed end wall.

II. APPARATUS

A. Vortex Tubes and Fluid-Supply Systems

The basic vortex tube, configuration (a), used for these experiments consisted of two concentric cylindrical steel tubes held together at both ends by flanges (Fig. 2). The annular space between the tubes served as a manifold that supplied the high-pressure gas or binary gas mixture to each of the 804 driving jet tubes. These jet tubes were fabricated of 0.062-in.-O.D. by 0.007-in.-I.D. stainless-steel tubing cut into 0.90-in. lengths and cemented into holes drilled through the wall of the inner tube. The overall effect of this arrangement was to have 0.007-in.-diam. jets arranged in a helix and tangent to a circle whose diameter was 92% of the inner-tube I.D. The helix contained six equally spaced jets per cycle and had a pitch of 0.180 in. This pattern of jets covered the entire inner cylindrical surface of the basic vortex tube, which was 24.14 in. long and 4.50 in. in diameter.

The mass flow rate of the hydrogen or nitrogen gas being continuously supplied to the vortex-tube manifold was measured with a choked venturi located in the supply line approximately 3 ft upstream of the manifold. The Freon-13 gas, obtained from a cylinder of liquified Freon-13 immersed in a water bath and held at approximately 100°F, was for most of the experiments injected into the hydrogen or nitrogen at the throat of a second venturi located in the manifold supply line downstream of the choked venturi and 16-in. upstream of the vortex-tube manifold. For several experiments, however, the Freon was injected directly into the vortex tube at the center of one end wall. In both Freon-injection schemes the mass flow rate was measured with one of three rotameters, depending on the value selected for the experiment. The flow was started and stopped with an electrical solenoid valve located at the point of injection.

The discharge of the vortex tube left through a nozzle located at the center of one end wall. This nozzle had a convergent contour radius and throat radius of 0.31 in. and a divergent expansion cone of 45-deg half-angle. The fluid then passed through a diffuser designed to reduce the swirl component of the velocity and to provide a steady, homogeneous flow in a constant-area rectangular duct 2.00 in. wide and 1.50 in. deep.

The second configuration used in this investigation, designated as configuration (b), is shown in Fig. 3. In configuration (b), the flow leaving the vortex tube through the end-wall nozzle was split into two coaxial streams by inserting a sharp-edged tube into the vortex through the nozzle throat with the edge extending 0.25 in. beyond the end-wall inner surface. The fluid exhausting through this 0.45-in.-I.D. tube was allowed to flow through the diffuser and constant-area duct. The remaining fluid, leaving the vortex tube through the annulus between the tube O.D. and the nozzle throat, was accumulated in a manifold and from there reinjected into the vortex at the center of the closed end wall. To accomplish this reinjection with as little disturbance to the vortex flow as possible, an injector that imparted a swirl to the injected fluid was used. The deflection of a tuft glued to the inner wall of this bypass system was taken as an indication that a flow existed between the exit orifice and the closed-end-wall injector.

The third configuration tested, configuration (c), was the same as configuration (b) except that a 4.50-in.-I.D. tube was inserted between and concentric with the basic vortex tube and the closed end wall, as shown in Fig. 4. This was done to increase the effective length of the vortex tube so that the reinjection binary mixture would have a longer path, and, hence, more time to lose its Freon. However, no means were provided for injecting fluid into the vortex through the cylindrical wall of this extension tube.

In addition to the three configurations described above, configuration (a) was used with two baffles installed inside the vortex chamber. These baffles were made of 0.75-in. aluminum angle, 24.0 in. long, and held firmly against the cylindrical wall at diametrically opposite points. In effect these baffles were like two fences, each protruding radially into the flow for approximately 0.75 in. over the entire length of the vortex tube, and were used to greatly reduce the swirl component of the flow.

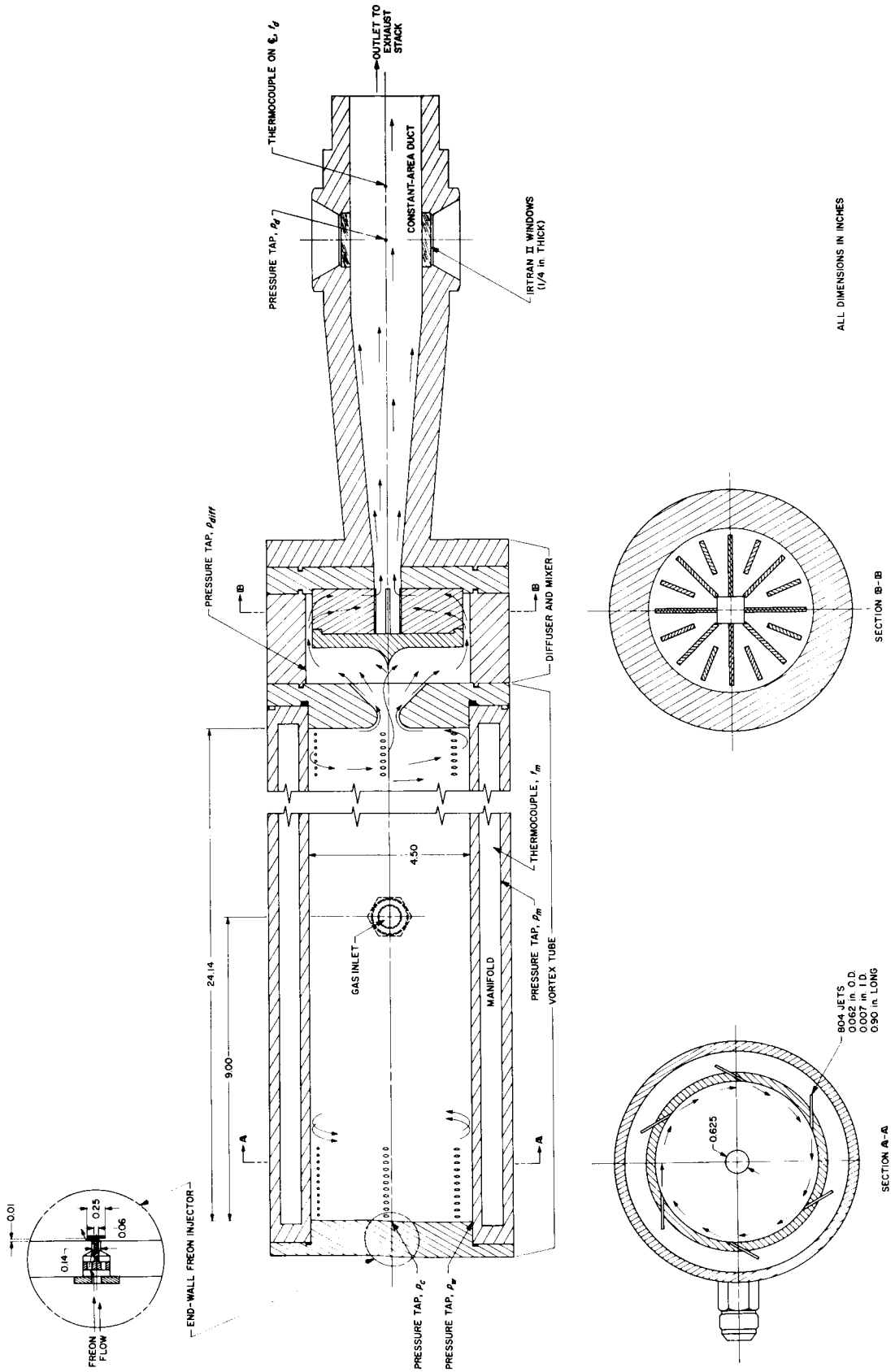

Fig. 2. Schematic of configuration (a)

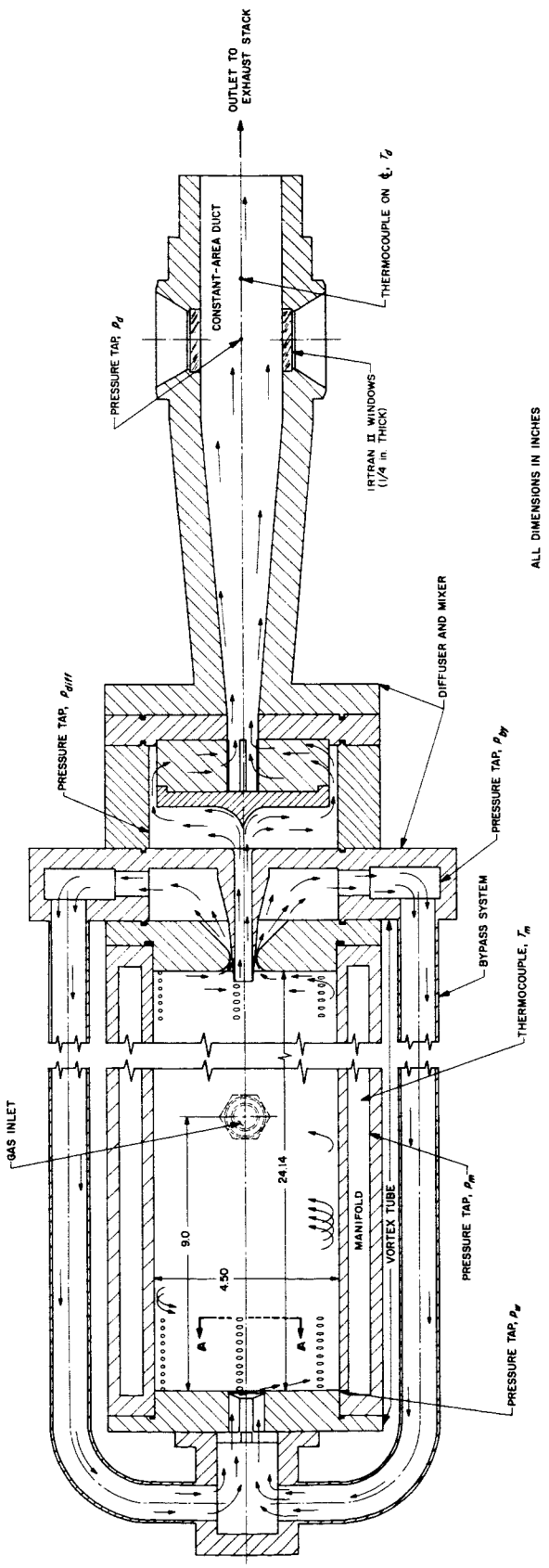

Fig. 3. Schematic of configuration (b)

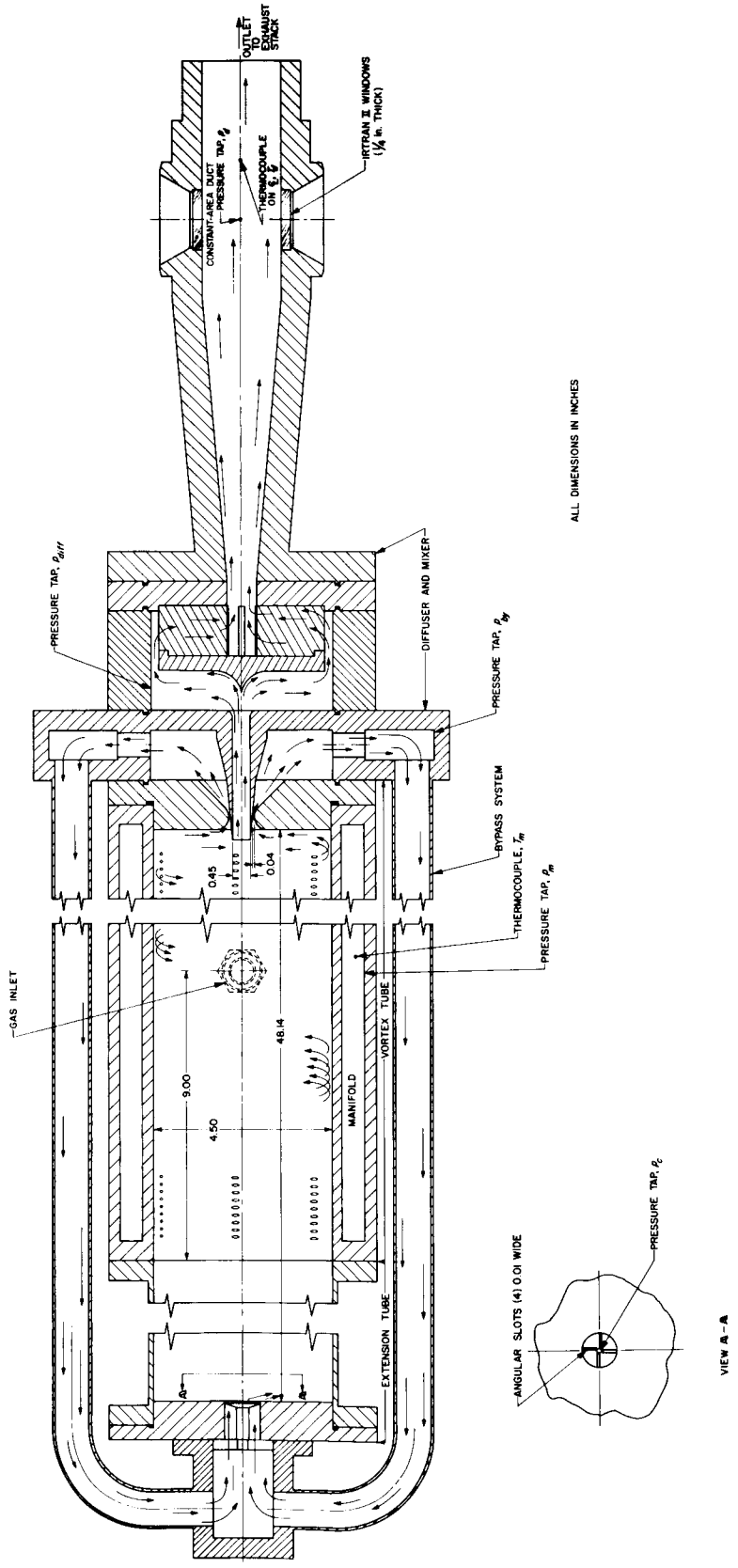

Fig. 4. Schematic of configuration (c)

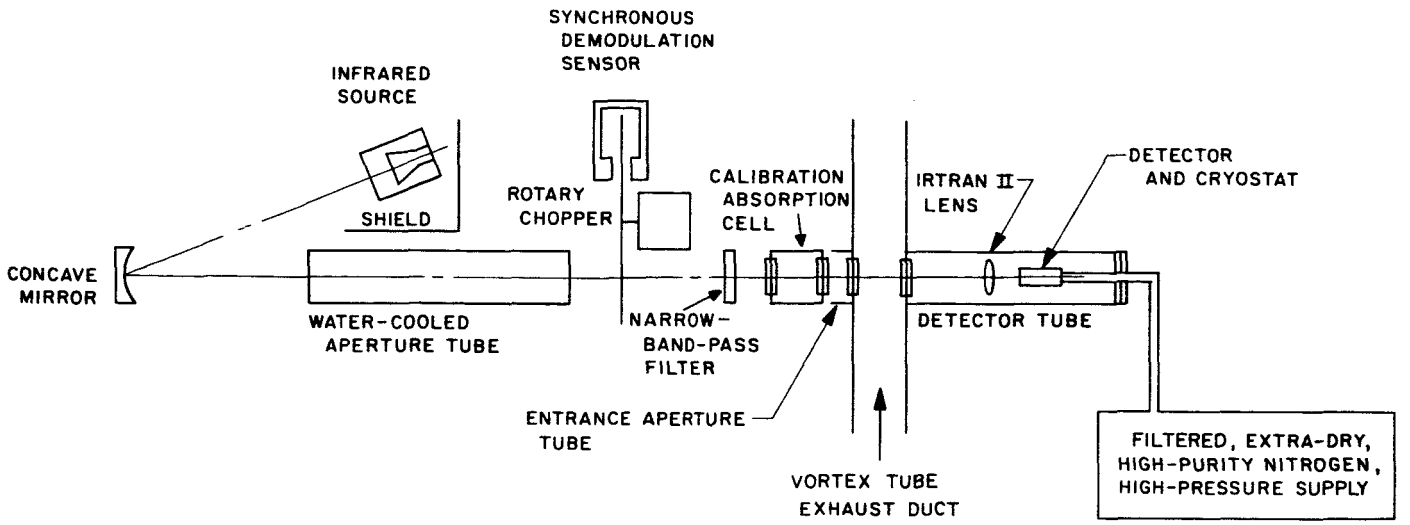

Fig. 5. Schematic of infrared photometer

B. Instrumentation

Copper-Constantan bare-wire thermocouples were used to measure the fluid temperature at the following four points: 15 in. upstream of the choked venturi, in the vortex tube manifold, the constant-area exhaust duct, and the discharge side of the Freon rotameters. Laboratory-type bourdon-tube pressure gauges were used to measure the stagnation pressure 15 in. upstream of the choked venturi, the manifold pressure, the cylindrical-wall static pressure, the centerline pressure at the closed end wall, the bypass system pressure for configurations (b) and (c), the diffuser pressure, and the Freon rotameter pressure. The static pressure in the constant-area exhaust duct was measured with an oil manometer.

An infrared photometer was developed and used to determine the Freon density, as a function of time, in the constant-area exhaust duct. A detailed description of the photometer and its associated electronics is given in Ref. 5. This photometer, shown schematically in Fig. 5, consisted of a ceramic infrared source, a collimating mirror, a rotary chopper that modulated the infrared beam at a frequency of 230 cps, a narrow-band-pass optical interference filter, a focusing lens, and a solid-state detector. All transmitting optical elements were made of Irtran II and the detector was a Philco GPC 201A gold-doped germanium type with a 2.0-mm-sq. germanium flake that was cooled with liquid nitrogen.

At room temperature and a pressure of the order of 1 cm Hg abs or less, the first strong absorption band for Freon-13 is centered at a wavelength of approximately 8.3μ. Therefore, in order to optimize the sensitivity of the photometer to changes in Freon partial pressure, an optical filter, which isolated a narrow band centered at approximately 8.3μ, was selected. A typical transmittance spectrum of Freon-13 and the transmittance spectrum of the optical filter used in this instrument are shown in Fig. 6. Since the filter transmittance band and Freon absorption band are not precisely centered at the same wavelength, as is shown in Fig. 6, it was necessary to rotate the filter so that the infrared beam would enter the element at an angle of 60 deg. Doing so shifted the filter transmittance band to a slightly lower wavelength.

The infrared-detector signal amplification system consisted of a high-gain, low-noise, band-pass amplifier, which amplified the modulation components of the infrared-detector output signal. This was followed by a synchronous demodulator, amplifier, and low-pass filter, which produced the electrical signal proportional to the infrared radiation incident on the detector. An attenuated, filtered output with a nominal signal level of +20 to +40 mv and a band pass of 1 cps was then fed to a strip-chart recorder that had a chart speed of 1.0 in./sec. A signal indicating the position of the Freon-controlling solenoid valve was also recorded on this same strip chart.

In addition to being recorded as a function of time, the infrared-detector output was integrated with respect to time. This was done by first adding the attenuated signal to a variable bucking voltage and then feeding this sum into a voltage-to-frequency (V-F) converter (Dymec, Model 2211BR). The bucking voltage was adjusted before each experiment so that the V-F converter would see zero volts when there was no Freon in the

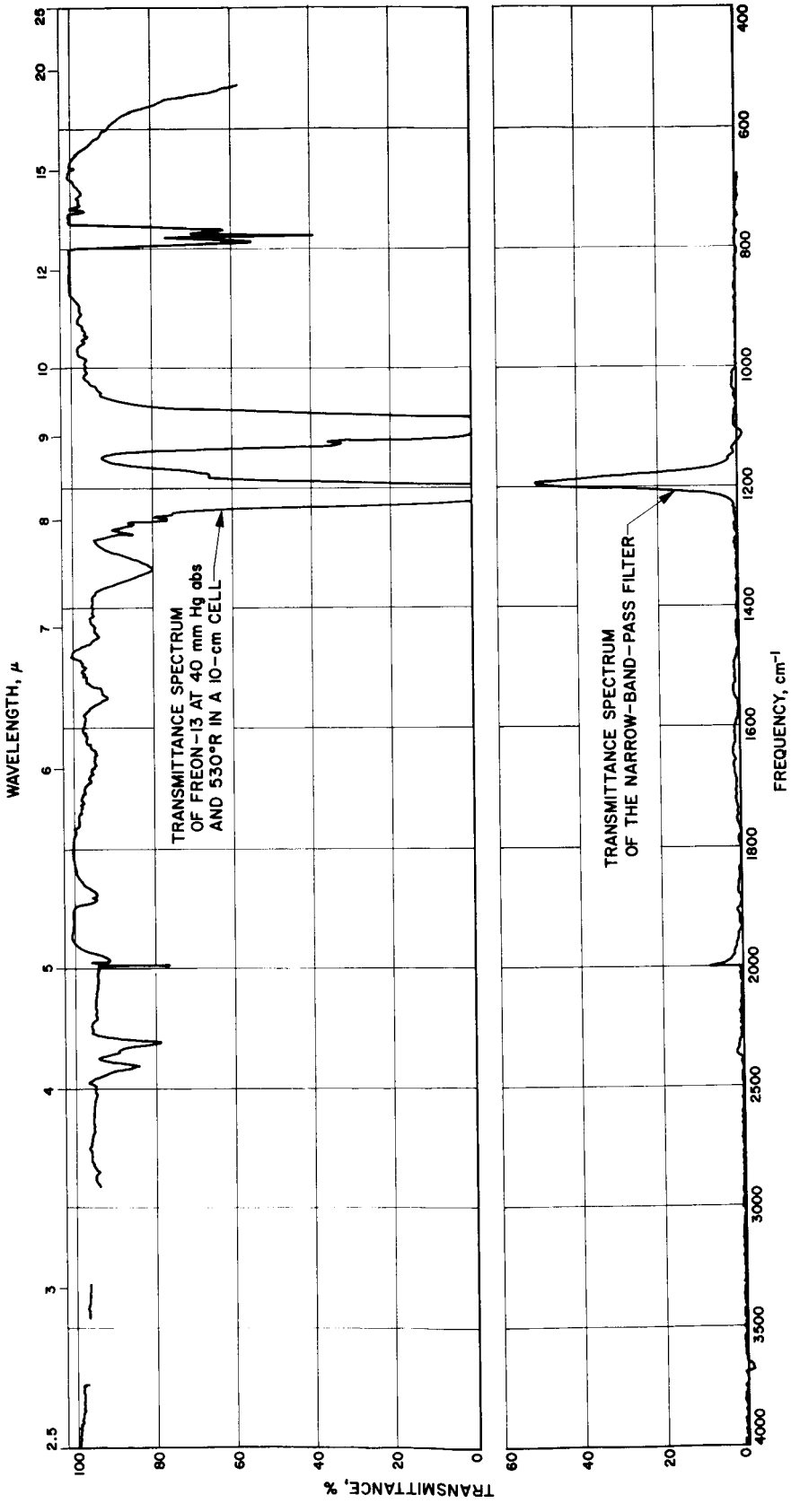

Fig. 6. Transmittance spectra of Freon-13 and optical interference filter

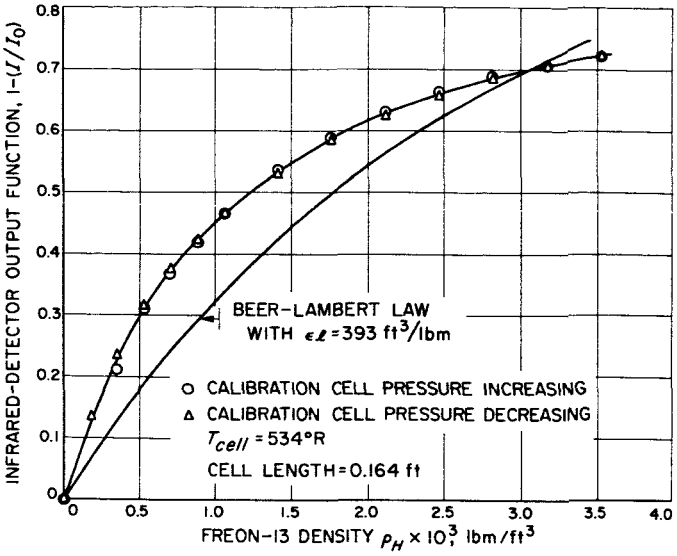

Fig. 7. Photometer calibration data

exhaust tube. The output of the V-F converter had a frequency proportional to the original infrared-detector output; hence by counting cycles with a computing digital indicator (Dymec, Model DY-2500), the time integral of the infrared-detector output was obtained. The computing digital indicator gate and the solenoid valve controlling the Freon flow into the experiment were wired together so that the counter gate would open the instant the Freon flow was stopped.

The photometer was calibrated with the aid of an absorption cell containing pure Freon-13 at room temperature and at various known pressures ranging from 0 to 1 cm Hg abs. This calibration cell duplicated, approximately, the optical path length of the constant-area exhaust duct and had Irtran II windows identical with those installed in the exhaust duct. An oil-filled micromanometer was used to measure the cell pressure. The calibration data are shown in Fig. 7 as a plot of the detector-output difference $I_0 - I$ normalized with respect to the output corresponding to zero Freon pressure or $1 - (I/I_0)$ vs Freon density ρ_H. The Freon density was computed from the largest term in the equation of state for Freon-13 given in Ref. 6. For Freon pressures less than 25 cm Hg abs, the error involved in neglecting the remaining terms is less than 0.5%. The approximate equation of state used was

$$\rho_H = 9.737 \frac{p}{T} \tag{1}$$

The deviation of the calibration data from the Beer-Lambert law for light absorption (also shown in Fig. 7) is probably due to the particular shape of the optical filter and Freon transmittance spectra.

III. TESTS

A typical experiment began by first establishing the steady-state flow of hydrogen or nitrogen through the vortex tube. This was done by opening a pneumatic valve in the supply line and increasing the pressure in the system, by adjusting two regulators in series, until the desired cylindrical-wall static pressure was reached. This pressure was measured at the closed end of the vortex tube. The solenoid valve controlling the Freon flow was then opened and the desired flow rate established by adjusting a needle valve located on the upstream side of the solenoid valve. After setting the needle valve, the Freon flow was momentarily shut off and all electrical and pneumatic functions checked for level and steadiness. Then the Freon flow was turned on again and all pressures, temperatures, the infrared-detector output, and the Freon flow rate were recorded during this period of steady-state operation. Also, since the Freon-controlling solenoid valve was open, the computing digital indicator gate was automatically closed and the register could be cleared and set to zero. The solenoid valve was then closed and after all traces of Freon had been purged, as evidenced by the infrared-detector output, the computing digital indicator gate was closed. In this manner a complete time trace of the Freon density in the exhaust tube, starting from several seconds before the Freon was turned on and ending several seconds after all Freon had been purged, was obtained. Also, the number locked in the computing digital indicator register was recorded.

IV. RESULTS

Two typical examples of the amplified infrared-detector output vs time traces are shown in Fig. 8 and 9. Both of these results were obtained in configuration (a) with a cylindrical-wall pressure p_w of 29.1 psia and a Freon-13 mass flow rate $\dot{m}_H$ of approximately 0.0012 lbm/sec. In Fig. 8 hydrogen was used as the principal species with a mass flow rate $\dot{m}_L$ of 0.0145 lbm/sec, while to obtain the results of Fig. 9, nitrogen was used with $\dot{m}_L = 0.0577$ lbm/sec. The initial overshoot of the detector output to values below steady state, which is evident in both Fig. 8 and 9, occurred at all conditions except for a few experiments made at high Freon and hydrogen or nitrogen flow rates. However, it appears that this overshoot has no connection with the rotational flow field since it also occurred when the baffles were installed in configuration (a). Hence, it is believed that the overshoot was caused by some dynamic characteristic of the Freon-injection system.

Although the steady-state Freon flow rate was approximately the same in the experiments of Fig. 8 and 9, the Freon density in the exhaust duct is higher for the nitrogen flow, as indicated by the lower steady-state infrared-detector output. This is due to the lower exhaust velocity that is characteristic of the nitrogen flow. By assuming that the two species have the same mean exhaust velocity in the duct (no diffusion) and the same temperature, the Freon density in the duct, obtained from the continuity equations and perfect gas equation of state, can be written as

$$\rho_{H_d} = \frac{p_d}{R_L T_d} \cdot \frac{\dot{m}_H}{\dot{m}_L} \left(\frac{1}{1 + \frac{R_H}{R_L} \frac{\dot{m}_H}{\dot{m}_L}} \right)$$

However, since the ratio of gas constants R_H/R_L is 0.019 and 0.268 for hydrogen and nitrogen, respectively, and the ratio of mass flow rates $\dot{m}_H/\dot{m}_L$ was nominally less than 0.1, the following approximation can be used for the Freon density in the exhaust duct:

$$\rho_{H_d} \simeq \frac{p_d}{R_L T_d} \times \frac{\dot{m}_H}{\dot{m}_L} \tag{2}$$

The fluid pressure p_d and temperature T_d in the exhaust duct were approximately constant and equal to ambient conditions for all experiments; therefore, the steady-state Freon density and hence the detector output depend mainly on the molecular weight and mass flow rate of the principal species and on the Freon mass flow rate.

The results obtained from the several experiments made at various Freon and hydrogen or nitrogen mass flow rates in the five vortex-tube configurations are listed in Tables 1 through 5. The measured fluid pressures and temperatures and the mass flow rates calculated from the choked venturi and rotameter data characterize the flow field. The time history of the Freon density in the exhaust duct is characterized by the relative infrared-detector output at the initial overshoot I_{min}/I_0 and during steady-state operation I_{st}/I_0, where I_0 is the detector output under conditions of zero Freon density in the exhaust duct. To characterize the transient behavior of the detector output after the Freon injection is stopped, the dead time l and time constant t' were used and are tabulated along with the computing digital indicator output $\mathcal{I}$, which is proportional to the integral $\int [1 - (I/I_0)]\, dt$. The dead time and time constant are defined in Fig. 10. The repeatability of $\mathcal{I}$ was found to be within approximately $\pm 1\%$ when $\mathcal{I}$ was greater than 10^4 and within approximately $\pm 5\%$ when $\mathcal{I}$ was less than 10^4.

From the data listed in Tables 1 through 5, an approximation of the mass of Freon m_H retained in the vortex tube (including the manifold and diffuser) during steady-state operation was calculated for each run and is also listed in Tables 1 through 5. This retained mass can be obtained by integrating the Freon mass flow rate leaving the vortex tube as a function of time, starting at the instant t_1 that the Freon injection into the device had been stopped and ending at t_2 when all the Freon had been purged from the system; hence

$$m_H = \int_{t_1}^{t_2} \dot{m}_H\, dt \tag{3}$$

Equation (2) provides an approximate expression for the Freon mass flow rate in terms of the Freon density, which is measured by the photometer, and quantities that are constant during an experiment. The Freon density is related to the infrared-detector output through the calibration curve of Fig. 7. However, a linear relationship between the Freon density and the detector output function $1 - (I/I_0)$ was assumed so that the electronic integral $\mathcal{I}$ could be used as a measure of the integral in Eq. (3).

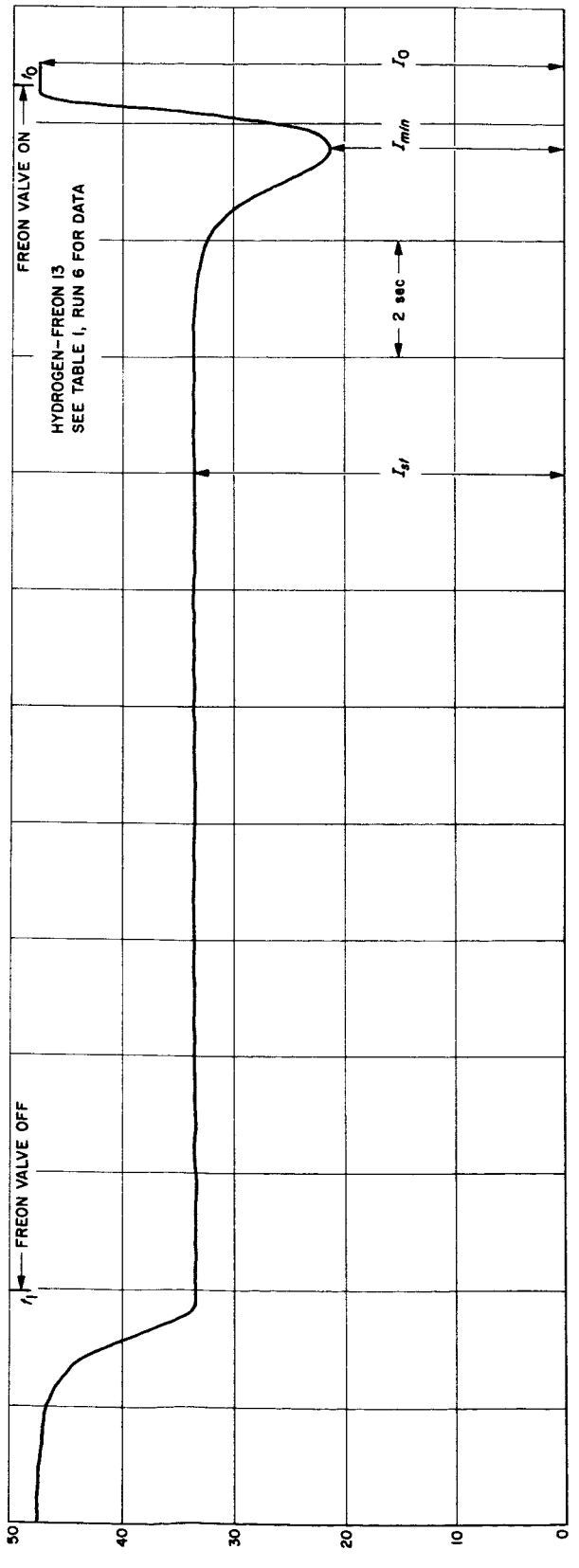

Fig. 8. Infrared-detector output vs time trace for Freon-hydrogen experiment

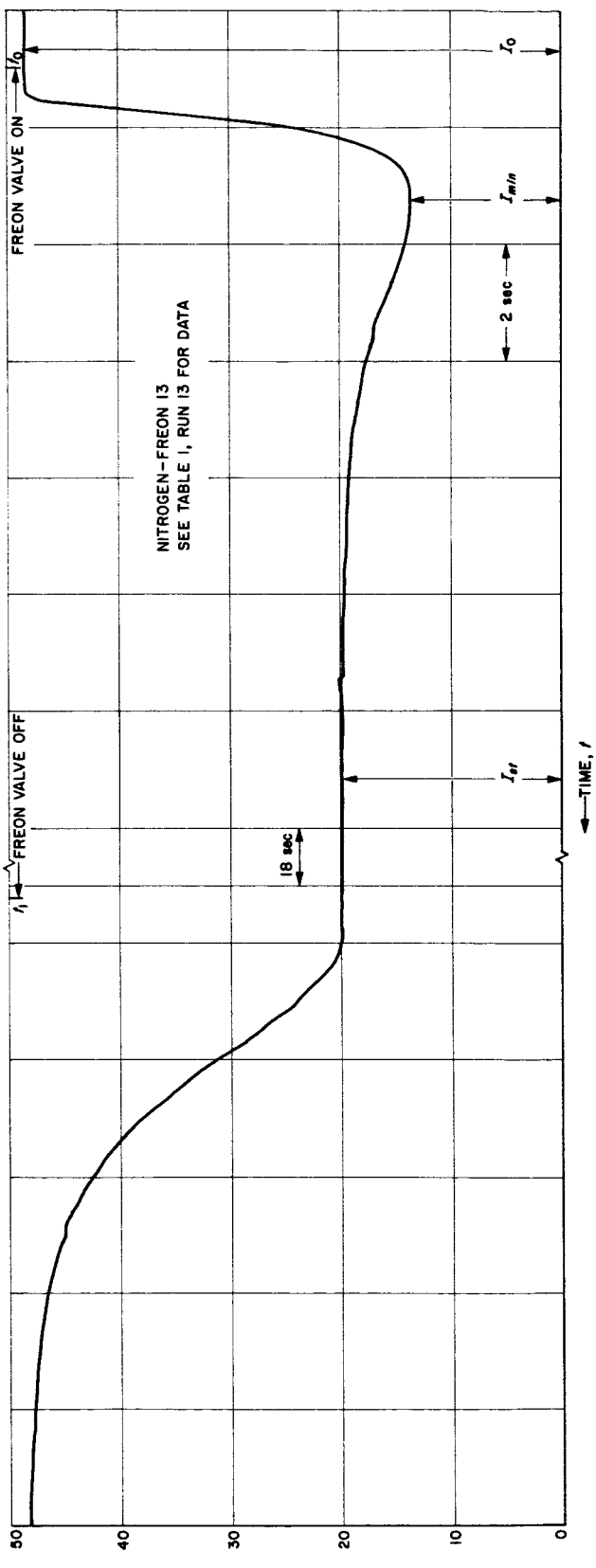

Fig. 9. Infrared-detector output vs time trace for Freon-nitrogen experiment

Table 1. Experimental results from configuration (a)
Ambient conditions: $p = 14.12$ psia, $T = 512°R$

Run	Fluid	p_m psia	T_m °R	p_w psia	p_c psia	p_{diff} psia	p_d psia	T_d °R	$\dot{m}_L$ lbm/sec	$\dot{m}_H$ lbm/sec	I_0 mv	I_{min}/I_0	I_{st}/I_0	l sec	t' sec	$\mathcal{J}$	m_H lbm	$m_H/[m_H]_{D_{LH}=0}$	τ sec
1	H_2	57.	509	19.1	9.6	14.1	14.11	510	0.00670	0.000133	47.3	0.447	0.888	0.41	0.64	5,030.	0.000120	1.25	0.903
2	H_2	58.	509	19.1			14.11	509	0.00670	0.000334	47.4	0.428	0.773	0.37	0.74	11,307.	0.000302	1.23	0.903
3	H_2	59.	509	19.1			14.11	509	0.00669	0.000541	47.4	0.357	0.682	0.40	0.72	16,092.	0.000495	1.23	0.916
4	H_2	126.	509	29.1	5.3	14.3	14.10	509	0.0149	0.000295	47.6	0.556	0.891	0.35	0.61	4,856.	0.000240	1.29	0.814
5	H_2	126.	509	29.1			14.10	509	0.0147	0.000718	47.5	0.503	0.782	0.36	0.65	10,653.	0.000635	1.38	0.885
6	H_2	128.	509	29.1			14.10	509	0.0145	0.00118	47.6	0.445	0.706	0.34	0.70	14,584.	0.00106	1.37	0.898
7	H_2	208.	509	44.1	3.3	14.8	14.10	509	0.0243	0.000442	47.7	0.674	0.903	0.37	0.60	3,653.	0.000302	1.10	0.681
8	H_2	209.	508	44.1			14.10	509	0.0240	0.00112	47.6	0.578	0.785	0.40	0.64	9,125.	0.000856	1.21	0.765
9	H_2	209.	508	44.1			14.10	508	0.0238	0.00177	47.6	0.525	0.713	0.36	0.65	13,378.	0.00149	1.33	0.844
10	H_2	419.	506	84.1	4.6	17.5	14.08	505	0.0492	0.000965	47.9	0.888	0.895	0.34	0.62	4,368.	0.000726	1.24	0.753
11	H_2	418.	503	84.1			14.08	502	0.0488	0.00237	48.0	0.777	0.785	0.35	0.61	9,305.	0.00185	1.27	0.780
12	N_2	57.	502	19.1	9.3	14.2	14.12	503	0.0257	0.000532	48.1	0.207	0.393	1.38	2.74	139,687.	0.00222	1.56	4.160
13	N_2	123.	500	29.1	5.0	14.3	14.11	496	0.0577	0.00120	48.2	0.282	0.412	1.25	2.47	116,863.	0.00431	1.58	3.595
14	N_2	198.	493	44.1	2.9	14.7	14.11	469	0.0881	0.00162	48.5	0.301	0.437	1.23	2.41	107,604.	0.00560	1.40	3.460

Table 2. Experimental results from configuration (a) with end-wall Freon injection
Ambient conditions: $p = 14.24$ psia, $T = 528°R$

Run	Fluid	p_m psia	T_m °R	p_w psia	p_{diff} psia	p_d psia	T_d °R	$\dot{m}_L$ lbm/sec	$\dot{m}_H$ lbm/sec	I_0 mv	I_{min}/I_0	I_{st}/I_0	l sec	t' sec	$\mathcal{J}$	m_H lbm	$m_H/[m_H]_{D_{LH}=0}$	τ sec
1	H_2	58.	529	19.2	14.2	14.23	531	0.00681	0.000330	46.4	0.425	0.771	0.17	0.21	4,070.	0.000106	1.40	0.322
2	H_2	58.	531	19.2		14.23	532	0.00680	0.000537	46.4	0.417	0.680	0.18	0.19	4,488.	0.000135	1.09	0.252
3	H_2	57.	528	19.2		14.23	530	0.00675	0.000126	46.4	0.425	0.895	0.15	0.22	1,111.	0.0000243	0.83	0.193
4	H_2	219.	538	44.2	14.9	14.22	539	0.0240	0.000443	46.5	0.653	0.902	0.14	0.21	4,658.	0.000382	6.75	0.862
5	H_2	213.	539	44.2		14.22	541	0.0240	0.00115	46.5	0.621	0.783	0.13	0.20	1,617.	0.000154	1.05	0.134
6	H_2	213.	540	44.2		14.22	541	0.0240	0.00184	46.4	0.584	0.713	0.16	0.19	1,904.	0.000221	0.94	0.120
7	H_2	425.	539	83.7	17.6	14.19	539	0.0488	0.00386	46.5	0.594	0.659	0.13	0.20	2,194.	0.000448	1.02	0.116
8	H_2	425.	531	84.2		14.19	531	0.0491	0.000943	46.4	0.739	0.900	0.13	0.20	824.	0.000140	1.29	0.149
9	H_2	425.	529	84.2		14.19	529	0.0493	0.00244	46.5	0.681	0.778	0.11	0.17	1,511.	0.000278	0.82	0.114

Table 3. Experimental results from configuration (a) with baffles installed
Ambient conditions: $p = 14.11$ psia, $T = 510°R$

Run	Fluid	p_m psia	T_m °R	p_w psia	p_c psia	p_d psia	T_d °R	$\dot{m}_L$ lbm/sec	$\dot{m}_H$ lbm/sec	I_0 mv	I_{min}/I_0	I_{st}/I_0	l sec	t' sec	$\mathcal{J}$	m_H lbm	$m_H/[m_H]_{D_{LH}=0}$	τ sec
1	H_2	55.	506	14.4	14.3	14.10	497	0.00672	0.000145	45.4	0.465	0.878	0.33	0.72	6,512.	0.000140	1.45	0.966
2	H_2	56.	506	14.4		14.10	497	0.00672	0.000334	45.5	0.453	0.772	0.31	0.76	11,317.	0.000300	1.33	0.900
3	H_2	57.	506	14.4		14.10	497	0.00672	0.000520	45.4	0.438	0.689	0.32	0.79	16,893.	0.000510	1.44	0.982
4	H_2	126.	506	15.6	15.5	14.10	497	0.0149	0.000255	45.3	0.583	0.917	0.37	0.60	4,269.	0.000234	1.58	0.920
5	H_2	128.	506	15.6		14.10	497	0.0149	0.000796	45.1	0.557	0.790	0.24	0.69	9,698.	0.000665	1.41	0.835
6	H_2	129.	506	15.6		14.10	496	0.0149	0.00118	45.3	0.516	0.722	0.23	0.75	12,375.	0.000951	1.35	0.805
7	H_2	208.	506	18.1	18.0	14.09	505	0.0244	0.000452	45.1	0.738	0.917	0.26	0.59	3,896.	0.000384	1.54	0.849
8	H_2	210.	505	17.9		14.09	506	0.0244	0.00111	45.4	0.659	0.796	0.26	0.71	7,898.	0.000778	1.27	0.700
9	H_2	204.	505	18.1		14.09	505	0.0239	0.00182	45.4	0.605	0.721	0.21	0.74	11,409.	0.00135	1.33	0.740
10	N_2	204.	503	17.6	17.5	14.10	501	0.0906	0.00182	45.4	0.430	0.430	0.50	3.05	98,917.	0.00571	1.55	3.140

Table 4. Experimental results from configuration (b)
Ambient conditions: $p = 13.75$ psia, $T = 528°R$

Run	Fluid	p_m psia	T_m °R	p_w psia	p_c psia	p_{by} psia	p_{diff} psia	p_d psia	T_d °R	$\dot{m}_L$ lbm/sec	$\dot{m}_H$ lbm/sec	I_0 mv	I_{min}/I_0	I_{st}/I_0	l sec	t' sec	$\mathcal{J}$	m_H lbm	$m_H/[m_H]_{D_{LH}=0}$	τ sec
1	H_2	39.	525	18.8				13.74	523	0.00395	0.000127	46.7	0.406	0.835	0.49	1.00	11,412.	0.000160	1.14	1.260
2	H_2	38.	529	18.8				13.74	524	0.00394	0.000348	46.6	0.389	0.671	0.52	0.97	25,404.	0.000486	1.28	1.398
3	H_2	39.	526	18.8				13.74	531	0.00393	0.000558	46.6	0.382	0.576	0.55	1.16	34,774.	0.000830	1.37	1.487
4	H_2	79.	528	28.8				13.74	528	0.00892	0.000299	46.5	0.539	0.846	0.45	0.80	8,735.	0.000306	1.24	1.023
5	H_2	79.	531	28.8				13.74	531	0.00872	0.000758	46.7	0.506	0.688	0.47	0.79	18,610.	0.000820	1.29	1.081
6	H_2	79.	533	28.8				13.74	533	0.00862	0.00121	46.5	0.486	0.612	0.47	0.85	23,966.	0.00135	1.33	1.118
7	H_2	129.	510	43.8				13.73	520	0.0147	0.000448	46.5	0.645	0.853	0.43	0.77	7,554.	0.000413	1.17	0.923
8	H_2	129.	527	43.8				13.73	525	0.0143	0.00116	46.5	0.591	0.694	0.47	0.78	17,029.	0.00117	1.25	1.008
9	H_2	130.	530	43.8				13.73	527	0.0142	0.00189	46.5	0.550	0.594	0.50	0.80	24,718.	0.00208	1.37	1.102
10	H_2	129.	537	43.8				13.73	535	0.0143	0.00101	46.5	0.610	0.734	0.45	0.74	14,455.	0.000992	1.24	0.982
11	H_2	130.	538	43.8				13.73	537	0.0137	0.00245	46.6	0.502	0.518	0.51	0.83	30,028.	0.00276	1.36	1.128
12	H_2	124.	539	43.8				13.73	538	0.0129	0.00394	46.6	0.385	0.385	0.58	0.98	44,924.	0.00521	1.56	1.321
13	N_2	36.	533	18.8	8.1	17.3	13.8	13.75	532	0.0141	0.000152	46.1	0.317	0.535	1.59	3.58	132,411.	0.000786	1.28	5.175
14	N_2	74.	531	28.8	5.4	24.6	13.8	13.75	529	0.0316	0.000299	46.0	0.419	0.576	1.41	2.68	94,931.	0.00121	1.31	4.055
15	N_2	125.	529	43.8	5.6	35.5	14.0	13.74	524	0.0534	0.000996	46.0	0.425	0.425	1.70	2.75	135,135.	0.00424	1.44	4.255
16	N_2	124.	526	43.8				13.74	521	0.0534	0.000457	46.2	0.521	0.603	1.42	2.43	81,344.	0.00169	1.25	3.703
17	N_2	123.	523	43.8				13.74	517	0.0530	0.00115	46.4	0.391	0.391	1.35	3.24	144,338.	0.00493	1.44	4.290
18	N_2	124.	522	43.8				13.74	514	0.0531	0.00189	46.4	0.332	0.332	1.64	3.50	172,393.	0.00883	1.56	4.665

Table 5. Experimental results from configuration (c)
Ambient conditions: p = 14.19 psia, T = 526°R

Run	Fluid	p_m psia	T_m °R	p_w psia	p_c psia	p_{by} psia	p_{diff} psia	p_d psia	T_d °R	$\dot{m}_L$ lbm/sec	$\dot{m}_H$ lbm/sec	I_0 mv	I_{min}/I_0	I_{st}/I_0	l sec	l' sec	$\mathcal{J}$	m_H lbm	$m_H/[m_H]_{D_{LH}=0}$	τ sec
1	H_2	89.	519	19.2				14.18	520	0.0105	0.000136	47.2	0.586	0.925	—	—	4,030.	0.000132	1.15	0.973
2	H_2	89.	526	19.2				14.18	528	0.0103	0.000348	47.1	0.571	0.840	0.38	0.77	9,057.	0.000356	1.20	1.023
3	H_2	89.	528	19.2				14.18	531	0.0103	0.000537	47.0	0.555	0.776	—	—	13,117.	0.000571	1.25	1.061
4	H_2	89.	538	19.2				14.18	539	0.0101	0.000537	46.8	0.558	0.777	0.40	0.80	12,268.	0.000534	1.17	0.995
5	H_2	91.	534	19.2				14.18	535	0.0104	0.000538	46.6	0.566	0.787	0.40	0.80	11,428.	0.000523	1.15	0.972
6	H_2	164.	539	29.2				14.17	540	0.0186	0.000298	46.6	0.734	0.921	0.38	0.75	4,325.	0.000295	1.30	0.991
7	H_2	164.	540	29.2				14.17	541	0.0184	0.000757	46.9	0.698	0.825	0.35	0.75	8,564.	0.000666	1.15	0.880
8	H_2	164.	540	29.2				14.17	540	0.0181	0.00119	46.6	0.677	0.772	0.34	0.78	12,930.	0.00122	1.30	1.028
9	H_2	253.	539	44.2				14.17	539	0.0274	0.000468	46.6	0.834	0.918	0.38	0.64	4,444.	0.000458	1.25	0.980
10	H_2	253.	537	44.2				14.17	538	0.0272	0.00115	46.6	0.780	0.818	0.38	0.70	9,506.	0.00109	1.19	0.945
11	H_2	251.	536	44.2				14.17	536	0.0270	0.00184	46.6	0.738	0.751	0.36	0.79	14,521.	0.00194	1.32	1.057
12	N_2	81.	527	19.2	9.1	18.8	14.2	14.19	527	0.0354	0.000558	47.1	0.431	0.461	1.40	3.15	141,724.	0.00266	1.45	4.760
13	N_2	153.	521	29.2	9.9	27.7	14.2	14.18	519	0.0671	0.00120	47.0	0.474	0.474	1.12	3.10	127,475.	0.00525	1.48	4.380
14	N_2	219.	513	44.2	14.2	41.5	14.2	14.18	508	0.102	0.00189	47.1	0.448	0.448	1.15	3.25	148,074.	0.00920	1.71	4.865

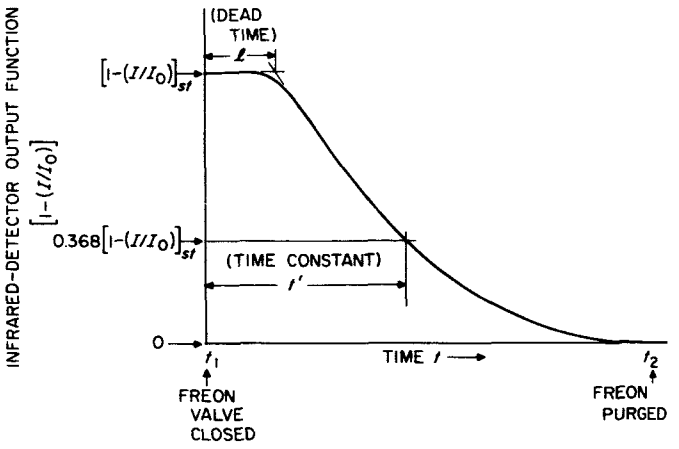

Fig. 10. Definition of dead time and time constant

The error involved in this assumption is computed, approximately, in the Appendix and shown to be less than 10% for all but five experiments. The error for runs 3, 6, and 9 of Table 4 is approximately 14%; 22% for run 11 of Table 4; and 39% for run 12 of Table 4. The relationship used was

$$\rho_{H_d} = C_0(1 - I/I_0) \tag{4}$$

and the constant of proportionality was taken as the ratio of the Freon density to the detector output function under steady-state operation:

$$C_0 \equiv \left[\frac{\rho_{H_d}}{1-(I/I_0)}\right]_{st} \tag{5}$$

By combining Eq. (2) through (5), an approximate expression for the mass of retained Freon in terms of the measured quantities is

$$m_H \simeq \left[\frac{\dot{m}_H}{1-(I/I_0)}\right]_{st} \int_{t_1}^{t_2}\left(1-\frac{I}{I_0}\right)dt = C_1\left[\frac{\dot{m}_H}{1-(I/I_0)}\right]_{st} \cdot \mathcal{J} \tag{6}$$

The constant C_1 is the scale factor relating the computing digital indicator output $\mathcal{J}$ (a nondimensional number) with the time integral of the transient detector output

$$\int_{t_1}^{t_2}\left(1-\frac{I}{I_0}\right)dt$$

This scale factor was determined by integrating seven selected time traces of the detector output between t_1 and t_2 with a planimeter and dividing by the corresponding value of $\mathcal{J}$. The average value of C_1 obtained in this way was 1.81×10^{-5} sec and the deviation from this average was found to be approximately $\pm 3\%$.

In order to evaluate the vortex-tube configurations as mass-retention devices, the ratio of m_H to the approximate Freon mass that would be contained if no diffusion occurred, $[m_H]_{D_{LH}=0}$, was computed and is listed in Tables 1 through 5. The contained mass is given by the integral of the Freon density over the entire volume of the device. By assuming that no diffusion occurs, the density ratio ρ_H/ρ_L can be taken as constant throughout the flow field and equal to the measured mass flow ratio $\dot{m}_H/\dot{m}_L$. Therefore

$$[m_H]_{D_{LH}=0} = \frac{\dot{m}_H}{\dot{m}_L}\int_V \rho_L\, dV \tag{7}$$

To evaluate the integral in Eq. (7), the flow was assumed to be isothermal with a temperature equal to that measured in the exhaust duct, T_d. Based on the radial temperature distribution measured in a similar vortex flow field (reported in Ref. 7), this assumption leads to an error of the order of 1% in the calculation of $[m_H]_{D_{LH}=0}$. Also, because the Freon mass flow rate is nominally less than 10% of the light-gas mass flow rate, the light-gas partial pressure is approximately equal to the total or measured pressure in the various parts of the system. Therefore, by adopting these approximations and using the equation of state for the light gas, the integral in Eq. (7) can be written as

$$\int_V \rho_L\, dV \simeq \frac{1}{R_L T_d}\{p_m V_m + \bar{p}_v V_v + p_d V_d + p_{by} V_{by}\} \tag{8}$$

The average pressure in the vortex tube proper $\bar{p}_v$ was obtained by graphically integrating the radial static-pressure distributions measured on the closed end wall of configuration (a). For these pressure measurements the diffuser and exhaust duct were absent and the end wall had a simple 0.625-in.-diam. hole at its center, with the fluid, nitrogen, discharging directly into the atmosphere. Details of these end-wall pressure measurements are discussed in Ref. 8. The normalized average static pressures $\bar{p}_v/p_w$ are shown as a function of the cylindrical-wall static pressure p_w in Fig. 11. Values of $\bar{p}_v$ were obtained from Fig. 11 for the results given in Tables 1, 2, 4, and 5. The average pressure in configurations (b) and (c) (Tables 4 and 5) must be higher than that given in Fig. 11 because of the difference in configuration, but the resulting error in the computed mass $[m_H]_{D_{LH}=0}$ is believed to be insignificant. For the results shown in Table 3 (configuration (a) with baffles), $\bar{p}_v$ was taken as the average between

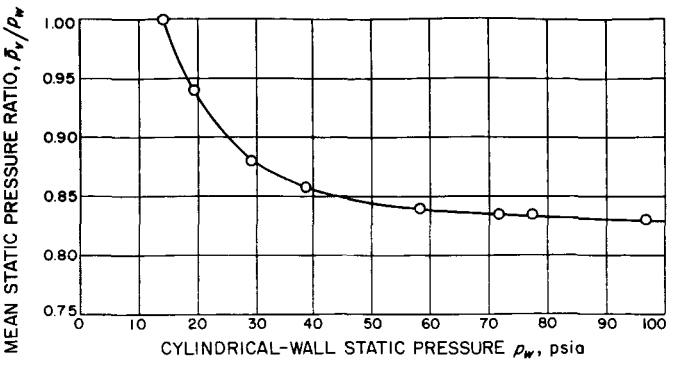

Fig. 11. Mean static pressure in compressible vortex flow fields

p_w and p_c. The internal volume of each chamber of the configurations, calculated from the nominal dimensions, is listed in Table 6, where V_d represents the total volume of diffuser, mixer, and constant-area duct out to the center of the Irtran windows.

The mass-retention time τ is here defined as the mass of heavy gas retained in the vortex during steady-state operation divided by the steady-state heavy-gas mass flow rate, or

$$\tau \equiv \left[\frac{m_H}{\dot{m}_H}\right]_{st} \tag{9}$$

An approximation of this mass-retention time was calculated for each run listed in Tables 1 through 5, by dividing Eq. (6) by the steady-state Freon mass flow rate. Note that the mass ratio $m_H/[m_H]_{D_{LH}=0}$ listed in Tables 1 through 5 is equal to the ratio $\tau/[\tau]_{D_{LH}=0}$.

The mass of Freon injected into the hydrogen flow during an entire run, $m_{H_{in}}$, was computed for several runs by assuming that the Freon mass flow rate reached the steady-state level at t_0, the instant the Freon-control valve was turned on, and that it dropped to zero at t_1, the instant the valve was closed; hence

$$m_{H_{in}} \simeq \dot{m}_{H_{st}}(t_1 - t_0) \tag{10}$$

Table 6. Internal volume of the various apparatus parts

Configuration (a)	Manifold volume, $V_m = 265$ in.^{3} Vortex tube volume, $V_v = 384$ in.^{3} Diffuser volume, $V_{diff} = 52$ in.^{3}
Configuration (a) with end wall Freon injection	Vortex tube volume, $V_v = 384$ in.^{3} Diffuser volume, $V_{diff} = 52$ in.^{3}
Configuration (a) with baffles	Manifold volume, $V_m = 265$ in.^{3} Vortex tube volume, $V_v = 365$ in.^{3} Diffuser volume, $V_{diff} = 52$ in.^{3}
Configuration (b)	Manifold volume, $V_m = 265$ in.^{3} Vortex tube volume, $V_v = 384$ in.^{3} Bypass system volume, $V_{by} = 176$ in.^{3} Diffuser volume, $V_{diff} = 52$ in.^{3}
Configuration (c)	Manifold volume, $V_m = 265$ in.^{3} Vortex tube volume, $V_v = 766$ in.^{3} Bypass system volume, $V_{by} = 243$ in.^{3} Diffuser volume, $V_{diff} = 52$ in.^{3}

Table 7. Computed total injected and exhausted Freon mass for five selected runs

Run	Ref. Table	$(t_1 - t_0)$ sec	$A\|_{t_0}^{t_2}$ sec	$m_{H_{in}}$ lbm	$m_{H_{in}}/m_{H_{out}}$
1	1	27.53	3.80	0.00366	0.812
3	1	28.05	9.71	0.0152	0.922
11	1	23.97	5.25	0.0568	0.982
14	1	28.31	18.0	0.0458	0.885
8	4	25.58	8.19	0.0297	0.958

This injected mass is compared in Table 7 with the total Freon mass $m_{H_{out}}$ that was exhausted from the vortex tube during the same run. The total exhausted mass was computed from an expression similar to Eq. (6), the difference being that the integration of the detector output function was made over the total time span of the run; hence

$$m_{H_{out}} \simeq \left[\frac{\dot{m}_H}{1 - (I/I_0)}\right]_{st} \int_{t_0}^{t_2} \left(1 - \frac{I}{I_0}\right) dt \tag{11}$$

These integrals were obtained graphically from time traces, such as those shown in Fig. 8 and 9, and are listed in Table 7 as $A\|_{t_0}^{t_2}$.

V. DISCUSSION

The primary objective of this investigation was to qualitatively determine the extent to which a strong vortex-type flow could increase the residence time of a high-molecular-weight gas relative to that of a second gas of much lower molecular weight in particular vortex-tube configurations. The flow of light gas tends to sweep the heavy gas out and, in principle, the radial pressure gradient, generated by the vortex-type flow, must prevent this by causing the heavy gas to diffuse away from the exhaust hole. A measure of the effectiveness of the vortex to retain a heavy gas was obtained by measuring the mass of Freon-13 retained in a vortex flow field of hydrogen or nitrogen gas and comparing this mass with what would be contained in the same device and under the same conditions of pressure and temperature if no diffusion occurred. The ratio $m_H/[m_H]_{D_{LH}=0}$ of retained mass to the contained mass if no diffusion occurred is given in Table 1 for the same configuration that was used to make detailed internal measurements of the radial and axial distributions of Freon-to-hydrogen and Freon-to-nitrogen mass-density ratios reported in Ref. 4. The retention time τ given in Table 1 can be interpreted as the time it takes for a mass of heavy gas equal to the retained mass to leak out of the device. As the mass ratio $m_H/[m_H]_{D_{LH}=0}$ is equal to the ratio of retention times $\tau/[\tau]_{D_{LH}=0}$, this ratio can be interpreted as the average residence time of a heavy-gas particle relative to the average residence time of that same particle if no diffusion occurred. For the Freon-hydrogen experiments, the retained mass, or average residence time, is approximately 10 to 38% greater than that expected if no diffusion occurred. Part and possibly all of this apparent excess mass or residence time can be attributed to the assumption that the Freon density in the exhaust duct is a linear function of the infrared-detector output function [see Eq. (4) and the Appendix]. The important conclusion to be drawn from these results is that vortex-tube configuration (a) does not significantly increase the average residence time of the heavy gas for the flow rates and pressure levels used in this investigation. This result reinforces the following conclusion drawn from the detailed measurements of the density-ratio distributions of Ref. 4 (an example of which is shown in Fig. 12): "Although the vortex-type flows that have been generated in the laboratory do affect the binary mixture in a way that is qualitatively predictable by a two-dimensional laminar theory, the effect is merely a perturbation of the homogeneous mixture and not the orders-of-magnitude alteration required by the gaseous-vortex-reactor concept."

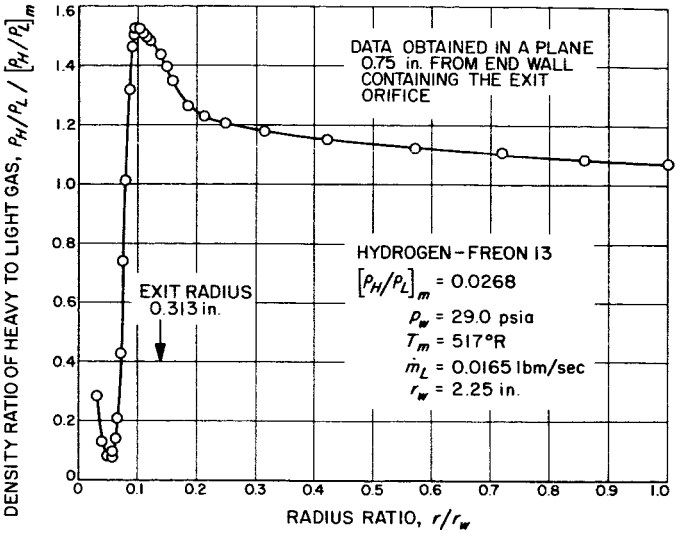

Fig. 12. Radial distribution of the heavy-gas to light-gas mass-density ratio

The result that the mass ratio $m_H/[m_H]_{D_{LH}=0}$ obtained for the Freon-nitrogen runs was greater than the corresponding runs made with Freon-hydrogen is again probably due to the error incurred when a linear relationship between Freon density and detector output function was assumed. The error in this case is larger because the Freon densities are higher than in the hydrogen runs (see Appendix).

As previously stated, the retention time τ can be interpreted as the time it takes for a mass of heavy gas equal to the retained mass to leak out of the device; hence, τ is equal to the average residence time for the heavy-gas particles. The gaseous-vortex-reactor concept requires a very large retention time if it is to be an economical system. For example, based on the parametric values assumed in the performance analysis of Ref. 1 (page 61, Case 3 with a beryllium oxide moderator), a retention time of 155 sec and a retained gaseous-fuel mass of 1.26×10^{-3} lbm per vortex tube (with a volume of 0.0103 ft^3) were required. The retention times calculated for the experiments performed in the basic vortex tube [configuration (a)] are listed in Table 1 and are seen to be of the order of 1 sec for the hydrogen experiments and between approximately 3 and 4 sec for the nitrogen experiments. The relatively large difference between the results for the nitrogen and hydrogen flows is due mostly to the fact that the nitrogen flows through the device at a much lower average velocity than does

the hydrogen. These low retention-time results are consistent with the conclusion that the diffusion rates generated in these vortex flows are not sufficient to materially alter the binary mixture.

One possible reason for the low values of retained mass, as determined by monitoring the heavy-gas mass flow rate out of the device after the heavy-gas valve is closed, is that part of the injected heavy gas might be trapped inside the vortex flow field. To check this possibility, the total mass of heavy gas injected into the vortex tube during an experiment was compared with the total mass exhausted from the tube during the same experiment, as determined from the photometer output. The ratio of injected to exhausted Freon $m_{H_{in}}/m_{H_{out}}$ was computed for five runs as shown in Table 7. The fact that the Freon mass exhausted from the vortex tube was found to be greater than that injected into the device is again due to the error incurred when a linear relationship between the Freon density and the infrared-detector output function was assumed (see Appendix). If a large mass of Freon were trapped, this ratio would be greater than 1. Since the five selected runs are believed to be representative of the entire set of experiments, it is believed that little or no Freon was trapped in the experiments of this investigation.

To evaluate the remaining configurations tested, the retention time τ and relative average residence time $\tau/[\tau]_{D_{LH}=0}$ were used, and are listed in Tables 2 through 5 as τ and $m_H/[m_H]_{D_{LH}=0}$. The data in Table 2 were obtained by injecting the Freon directly into configuration (a) through an orifice located at the center of the closed end wall. It was hoped that as this injected Freon flowed toward the exit hole it would be diffused radially outward to radii greater than that of the exit hole so that a part of this Freon would be retained in the vortex flow field. Detailed measurements of the Freon-to-hydrogen density ratio made in a similar configuration and reported in Ref. 4 indicate that the Freon does diffuse outward; however, the low relative residence times shown in Table 2 show that little or no Freon is retained by diffusion. Hence, one can conclude that the diffusion rates generated by these vortex flows are too small to have a significant effect on the average residence time. The fact that the retention times measured with end-wall injection are smaller than the corresponding ones measured with premixed fluids (Table 1) is due to the absence of Freon in the vortex-tube manifold and at the larger radii in the vortex tube proper when the Freon is injected at the end wall. The retention time computed for run 4, Table 2, is considerably larger than the rest; this is due, it is believed, to an error in the computing digital indicator output.

The data obtained with the baffles installed in configuration (a) are shown in Table 3. The effectiveness of the baffles to reduce the rotational mode of the flow field is demonstrated by the small difference between the cylindrical wall pressure p_w and the centerline pressure p_c. The relative average residence times computed for this configuration are approximately the same as those in Table 1. This is a further indication that the vortex generated in configuration (a) does not retain a significant amount of Freon through the process of binary diffusion.

The detailed measurements of the distribution of the mass-density ratio of heavy gas to light gas reported in Ref. 4 (an example of which is shown in Fig. 12) suggest that the binary mixture in the exit orifice of the vortex tube is rich in heavy gas near the periphery and lean near the center. For this reason configuration (b) was built, in which the exhausting jet was split into two concentric streams. The center stream was allowed to exhaust from the device through the diffuser and constant-area duct, while the peripheral stream was ducted back to the closed end of the vortex tube and the binary mixture reinjected into the vortex flow field at the center of the closed end wall. The injector imparted some swirl to this fluid in order to minimize its impact on the primary vortex flow. It was believed that as the reinjected fluid spiraled along the centerline toward the exit hole, some of the Freon would be diffused radially outward and the mass of Freon retained in the device would increase. The computed relative average residence times of the heavy gas in configuration (b), listed in Table 4, are approximately equal to the corresponding times obtained for the basic vortex tube (Table 1). However, because of the larger volume of the bypass system of configuration (b), the retention times for this configuration are slightly greater than those of configuration (a). Comparison of Tables 1 and 4 also shows that the light-gas mass flow rate $\dot{m}_L$ in configuration (b) is approximately one-half that in configuration (a) for the same wall pressure p_w. This is due to the fact that the effective exit-hole diameter in configuration (b) is smaller than in configuration (a).

The data obtained from configuration (c) (Fig. 4) are given in Table 5, in which the computed relative average residence times are again approximately equal to those of configuration (b), and the retention times τ less than those of configuration (b). The reduced retention time is probably caused by the increased light-gas mass flow

rate necessary to achieve the same wall pressure attained in configuration (b). Apparently the extension tube greatly increased the capacity of the boundary layer on the closed end wall for shunting fluid radially inward, thereby greatly reducing the relative vortex strength. To reduce the shunting effect the extension tube should have driving jets similar to those used for injecting the light gas into the vortex tube proper.

VI. CONCLUSION

The mass of Freon-13 retained in a binary compressible vortex flow field has been measured in several vortex-tube configurations and for several mass flow rates of Freon and hydrogen or nitrogen. The primary vortex-tube configuration used was the same as that used in a previous investigation in which measurements were made of the radial and axial distributions of the mass-density ratio of heavy gas to light gas (Ref. 4). It is concluded from the results of the present investigation that the average residence time of the Freon particles and the mass of Freon retained by all the configurations tested are approximately the same as they would be if no diffusion occurred in these flows. This conclusion is consistent with the results of Ref. 4, which show that the binary mixture is affected by the radial pressure gradient, but that this effect is merely a perturbation of the otherwise homogeneous mixture and not the orders-of-magnitude alteration required by the gaseous-vortex-reactor concept.

NOMENCLATURE

$A\big|_{t_0}^{t_2}$ value of $\int_{t_0}^{t_2} [1 - (I/I_0)]\, dt$, obtained graphically, sec

C_0 constant of proportionality between ρ_H and $[1 - (I/I_0)]$, lbm/ft³

C_1 scale factor relating $\mathcal{J}$ to $\int_{t_1}^{t_2} [1 - (I/I_0)]\, dt$, sec

D_{LH} binary diffusion coefficient, ft²/sec

e integrator error, %

I amplified infrared-detector output, mv

I_0 amplified infrared-detector output for zero Freon density, mv

I_{min} amplified infrared-detector output for maximum Freon density, mv

$[1 - (I/I_0)]$ infrared-detector output function

$\mathcal{J}$ computing digital indicator output

l dead time, sec, or path length, ft

m mass, lbm

$\dot{m}$ mass flow rate, lbm/sec

p static pressure, lbf/in.²

$\bar{p}_r$ mean static pressure in vortex tube proper, lbf/in.²

r radial coordinate, ft

R gas constant, ft-lbf/lbm °R

T temperature, °R

t time, sec

t' time constant, sec

V volume, in.³, or tangential velocity, ft/sec

ε absorption coefficient, ft²/lbm

ρ mass density, lbm/ft³

NOMENCLATURE (Cont'd)

$\Delta\rho_H$ maximum deviation from linear distribution, lbm/ft^3

τ retention time and average residence time, defined by Eq. (9), sec

Subscripts

0 conditions at instant Freon valve is opened

1 conditions at instant Freon valve is closed

2 conditions at instant all Freon is purged from system

by refers to bypass system of configurations (b) and (c)

c centerline

d refers to constant-area duct

diff refers to diffuser

H heavy gas (Freon-13)

in quantity injected into device

L light gas (hydrogen or nitrogen)

m manifold

out quantity exhausted from device

st steady-state conditions

v vortex tube proper

w cylindrical wall of vortex tube proper

REFERENCES

1. Kerrebrock, J. L. and Meghreblian, R. V., *An Analysis of Vortex Tubes for Combined Gas-Phase Fission-Heating and Separation of the Fissionable Material*, ORNL CF-57-11-3 Rev. 1, Oak Ridge National Laboratory, Oak Ridge, Tenn., April 11, 1958, declassified December 22, 1959. See also: Kerrebrock, J. L., and Meghreblian, R. V., "Vortex Containment for the Gaseous-Fission Rocket," *Journal of Aerospace Sciences*, Vol. 28, No. 9, September 1961.

2. Meghreblian, R. V., *Fuel-Containment Requirements for Gaseous-Fuel Nuclear Rockets*, Technical Report No. 32-441, Jet Propulsion Laboratory, Pasadena, Calif., September 2, 1963.

3. Keyes, Jr., J. J., and Dial, R. E., *An Experimental Study of Vortex Flow for Application to Gas-Phase Fission Heating*, ORNL-2837, C-86 Nuclear Rocket and Ram Jet Engines, Oak Ridge National Laboratory, Oak Ridge, Tennessee, June 13, 1960.

4. Pivirotto, T. J., *An Experimental and Analytical Investigation of Concentration Ratio Distributions In a Binary Compressible Vortex Flow*, Technical Report No. 32-808, Jet Propulsion Laboratory, Pasadena, Calif., March 15, 1966.

5. Wiker, G. A., and Willson, R. C., "An Infrared Photometer for Measuring Freon 13 Density in the Exhaust of a Hydrogen-Freon 13 Gas Core Reactor Model," *Space Programs Summary No. 37-32*, Vol. IV, Jet Propulsion Laboratory, Pasadena, Calif., April 30, 1965.

6. *Thermodynamic Properties of Freon-13 Refrigerant (Monoclorotrifluoromethane)*, Copyright 1959, E. I. du Pont de Nemours & Co., Inc., Wilmington, Dela.

REFERENCES (Cont'd)

7. Massier, P. F., "Axisymmetric Steady Flow of a Swirling Compressible Fluid Through a Convergent-Divergent Nozzle Without External Heat Transfer," *Space Programs Summary No. 37-33*, Vol. IV, Jet Propulsion Laboratory, Pasadena, California, June 30, 1965.

8. Pivirotto, T. J., *Radial Static Pressure Distributions in Confined Compressible Vortex Flow Fields*, Jet Propulsion Laboratory, Pasadena, Calif., (to be published).

APPENDIX

Integrator Error Analysis

To calculate the mass of Freon-13 retained in a vortex tube, the time integral of the Freon density in the exhaust stream is required. An approximation of this integral was obtained in this investigation by electronically integrating the infrared-detector output function with respect to time. An error is incurred in doing this because the Freon density and detector output function are not linearly related.

The calibration curve (Fig. 7) will be approximated for this analysis by a linear term plus a correction, or

$$\rho_H = \left[\frac{\rho_H}{1-(I/I_0)}\right]_{st}\left(1-\frac{I}{I_0}\right) - \Delta\rho_H \sin\frac{\pi}{[1-(I/I_0)]_{st}}\left(1-\frac{I}{I_0}\right) \tag{12}$$

The error is defined as

$$e = \left\{1 - \frac{C_0\int_{t_1}^{t_2}[1-(I/I_0)]\,dt}{\int_{t_1}^{t_2}\rho_H\,dt}\right\}\times 100 \tag{13}$$

where

$$C_0 \equiv \left[\frac{\rho_H}{1-(I/I_0)}\right]_{st}$$

Also, for this analysis, the transient distribution of the infrared-detector output function between t_1 and t_2, as shown in Fig. 8 and 9, will be approximated by a linear distribution, or

$$\left(1-\frac{I}{I_0}\right) = \left(1-\frac{I}{I_0}\right)_{st} - \frac{[1-(I/I_0)]_{st}}{(t_2-t_1)}\,t \tag{14}$$

By performing the indicated integrations in Eq. (13) with substitutions from Eq. (12) and (14) letting $t_1 = 0$, we get for the integrating error

$$e = \left\{\frac{1}{1-(\pi\rho_{H_{st}}/4\Delta\rho_H)}\right\}\times 100 \tag{15}$$

The maximum deviation from the assumed linear calibration curve, $\Delta\rho_H$, was graphically determined from Fig. 7 as a function of $\rho_{H_{st}}$ and these data were used to compute the approximate integrating error incurred for each $\rho_{H_{st}}$. The error distribution is shown in Fig. A-1. The error is negative because the assumed linear relationship between the Freon density and the detector output function results in an over-estimation of the retained Freon mass. The ratio of heavy-gas mass flow to light-gas mass flow corresponding to the steady-state Freon density in the exhaust duct, shown in Fig. A-1, was computed from Eq. (2) using $p_d = 14.1$ psia, $T_d = 530°$R, and $R_L = 766.8$ ft lbf/lbm °R. Note that for most hydrogen-Freon experiments the mass-flow ratio was less than 0.1; hence the integrating error was probably of the order of 10% or less.

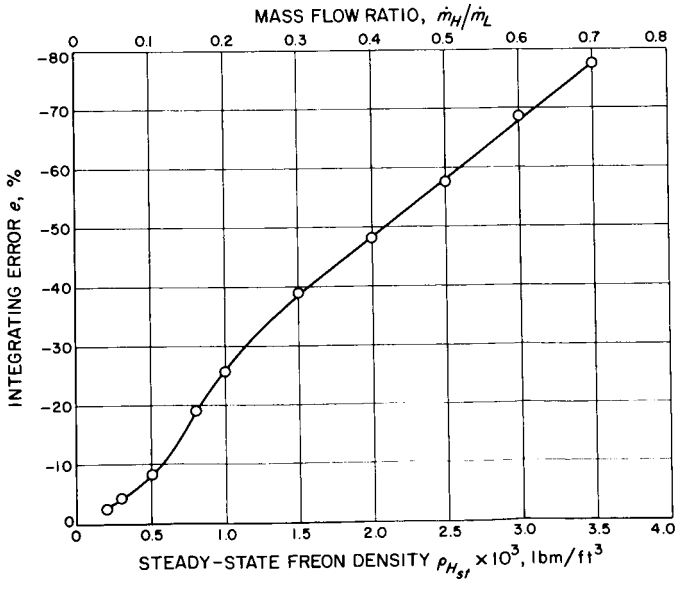

Fig. A-1. Results of integrator error analysis

ACKNOWLEDGMENT

The author is indebted to R. C. Willson, G. A. Wiker, and D. C. Griffin, Jr., for the design, development, and calibration of the infrared photometer used in this investigation.